Bacteriophytochrome from Magnetospirillum magneticum affects phototactic behavior in response to light

Haitao Chen, Dandan Li, Yao Cai, Long-Fei Wu, Tao Song

Bacteriophytochrome from *Magnetospirillum magneticum* affects phototactic behaviour in response to light

Haitao Chen[1,2,3], Dandan Li [5], Yao Cai[6], Long-Fei Wu[4,7 *], Tao Song[1,2,3 *]

[1] Beijing Key Laboratory of Biological Electromagnetism, Institute of Electrical Engineering, Chinese Academy of Sciences, Beijing 100190, China;

[2] University of Chinese Academy of Sciences, Beijing 100049, China;

[3] France-China International Laboratory of Evolution and Development of Magnetotactic Multicellular Organisms, Chinese Academy of Sciences, Beijing 100190;

[4] France-China International Laboratory of Evolution and Development of Magnetotactic Multicellular Organisms, CNRS, F-13402 Marseille, France;

[5] National Institute of Biological Sciences, Beijing 102206, China;

[6] Key Laboratory of Earth and Planetary Physics, Institute of Geology and Geophysics, Chinese Academy of Sciences, Beijing 100029, China;

[7] Aix Marseille University, CNRS, LCB, Marseille F-13402, France.

* Correspondences:

Dr. Long-Fei Wu

wu@imm.cnrs.fr

Dr. Tao Song

songtao@mail.iee.ac.cn

Tel. 86-10-82547164;

Fax 86-10-82547164.

Abstract

Phytochromes are a class of photoreceptors found in plants and in some fungi, cyanobacteria, photoautotrophic, and heterotrophic bacteria. Although phytochromes have been structurally characterized in some bacteria, its biological and ecological roles in magnetotactic bacteria remain unexplored. Here, we describe the biochemical characterization of recombinant bacteriophytochrome (BphP) from magnetotactic bacteria *Magnetospirillum magneticum* AMB-1 (*Mm*BphP). The recombinant *Mm*BphP displays all the characteristic features, including the property of binding to biliverdin (BV), of a genuine phytochrome. Site-directed mutagenesis identified that cysteine-14 is important for chromophore covalent binding and photoreversibility. Arginine-240 and histidine-246 play key roles in binding to BV. The N-terminal photosensory core domain of *Mm*BphP lacking the C-terminus found in other phytochromes is sufficient to exhibit the characteristic red/far-red-light-induced fast photoreversibility of phytochromes. Moreover, our results showed *Mm*BphP is involved in the phototactic response, suggesting its conservative role as stress-protective. This finding provided us a better understanding of the physiological function of this group of photoreceptors and photoresponse of magnetotactic bacteria.

Key words: Bacteriophytochrome, magnetotactic bacteria, biliverdin, phototactic behaviour.

Introduction

Light is an important environmental signal and provides sensory information for adaptation and energy for growth and metabolism. Protein-based photoreceptors have evolved to sense light quality changes in the environment and trigger critical lifestyle adaptations (Gomelsky and Hoff 2011; Gourinchas et al. 2019; Maresca et al. 2019). Phytochromes, which sense ambient light quality and quantity by responding to red and far-red light, are photoreceptor proteins used by bacteria, fungi, algae, and plants (Duanmu et al. 2014; Nagano 2016; Rodriguez-Romero et al. 2010). Phylogenetic analysis indicates that the phytochrome superfamily consists of five distinct clades, namely, plant phytochromes, cyanobacterial phytochromes, bacteriophytochromes (BphPs), fungal phytochromes, and a cluster of Phy-like sequences (Blumenstein et al. 2005; Hughes et al. 1997; Jaubert et al. 2008; Jiang et al. 1999; Karniol et al. 2005).

Most of bacteriophytochromes (BphPs) use a linear tetrapyrrole chromophore (biliverdin, BV) and sense red and far-red light via a reversible shift from a red-absorbing form (Pr) to a far-red-absorbing form (Pfr) (Rottwinkel et al. 2010; Vuillet et al. 2007). BphPs are composed of an N-terminal photosensory core domain (PCD) and a C-terminal output-transducing domain (OTD). The PCD comprises the period/aryl hydrocarbon receptor nuclear translocator/single-minded (PAS) that covalently binds to the open-chain BV chromophore via a thioether linkage with a conserved cysteine (Cys) residue, a cGMP phosphodiesterase/adenylyl cyclase/FhlA (GAF) domain stabilizing chromophore via polar and hydrophobic interactions, and a phytochrome-specific (PHY) domain stabilizing the photoactivated Pfr state (Burgie et al. 2016; Gourinchas et al. 2019; Lamparter et al. 2004). Upon light illumination, the PHY-tongue element undergoes partial refolding into an α-helix after chromophore photoisomerization (Burgie et al. 2016; Gourinchas et al. 2019). These structural rearrangements around a chromophore binding site transduce the molecular signal to a downstream effector module via the PHY domain and its C-terminal OTD (Bjorling et al. 2016; Gourinchas et al. 2019).

The C-terminal OTD of most BphPs possesses a two-component histidine kinase motif that transfers phosphate to a response regulator (RR) (Gourinchas et al. 2019; Jaubert et al. 2007; Karniol and Vierstra 2004; Rottwinkel et al. 2010). Other output modules, such as the PAS, GGDEF and EAL domains, which are involved in bacterial second messenger metabolism, have also been described (Rockwell et al. 2006). BphP in *Bradyrhizobium* ORS278 (*Br*BphP3) is formed from only N-terminal PCD without the C-terminal OTD. *Br*BphP3's feauture lies in its binding to phycocyano-bilin rather than BV, and it has been acquired by lateral gene transfer from a cyanobacterial species (Jaubert et al. 2007). The functional roles of this BphPs that lack the C-terminal OTD have yet to be found. The analysis of magnetotactic bacteria (MTB) genomes reveals some BphP photoreceptors (Brutesco et al. 2017; Wang et al. 2019), but only one BphP protein without a recognizable C-terminal OTD is found in the AMB-1 model strain of *Magnetospirillum*. MTB can synthesize intracellular magnetic crystals (magnetosomes) that allow cells to swim along geomagnetic field lines (Faivre and Schüler 2008; Frankel and Blakemore 1989;). This magnetotaxis of MTB can be dated back in the archean era, suggesting that MTB coevolved with the geomagneticfield over geological time (Lin et al. 2017). Interestingly, these bacteria are rich in light perception systems. Frankel et al. (1997) found that the *Magnetococcus* strain MC-1 has a negative photoresponse behaviour to short-wavelength light. Multicellular magnetotactic prokaryotes present a photophobic response and a photokinesis behaviour (Chen et al. 2015; de Melo and Acosta-Avalos 2017; Qian et al. 2019; Shapiro et al. 2011; Zhou et al. 2012). Illumination helps cell to eliminate intracellular reactive oxygen species (ROS) and triggers swimming toward a light source in *Magnetospirillum magneticum* AMB-1 (Chen et al. 2011; Li et al. 2017). Although the biological roles of BphPs have been addressed in some literatures (Bai et al. 2016; Bonomi et al. 2016; Moyano et al. 2020; Mukherjee et al. 2019; Ricci et al. 2015; Wu et al. 2013), the mechanism and biological function by which MTB respond to illumination remains unknown. Accordingly, we determined whether the BphP of MTB is involved in the regulation of photoresponse of this bacterium. By combining genetics, biochemical and biophysical approaches, we found that BphP in AMB-1 (*Mm*BphP) possesses red/far-red-light-

induced photochemical properties and participates in phototactic behaviour.

Materials and methods

Strain and culture conditions

M. magneticum AMB-1 strains (ATCC 700264) were grown under microaerobic condition on *Magnetospirillum* growth medium at 30°C (Chen et al. 2018; Matsunaga et al. 1991; Yang et al. 2001). *Escherichia coli* strains BL21 (DE3) (Tiangen, China) and WM3064 (Philippe and Wu 2010: 309-22) were grown in a LB medium at 37°C. When appropriate, AMB-1 was grown with 15 μg/mL apramycin or kanamycin. *E. coli* cultures were supplemented with apramycin (50 μg/mL) or kanamycin (50 μg/mL).

Identification of *Mm*BphP sequence

BphP was identified in the AMB-1 genomic database BLAST (protein accession number: WP_043744962.1). Phytochrome homologs were found with PDB 6FHT as a template (Jaubert et al. 2007). The domain was analyzed using SMART (http://smart.embl-heidelberg.de). For structural prediction, the protein sequence was examined using the Phyre2 program (http://www.sbg.bio.ic.ac.uk/phyre2/html/) (Kelley et al. 2015). Images were generated using AutoDock and PyMOL.

Cloning, expression, and purification of *Mm*BphP

The sequence of *Mm*BphP was PCR-amplified by using primers designed to introduce *BamH*I and *Xho*I sites before ATG and designated stop codons, respectively. The fragment was then cloned into the pET28a plasmid with N-terminal His6-SUMO-tagged fusion proteins. C14A, D197A, C211A, R240A, H246A, Y249A, S260A, C275A, H276A, C291A, C14&R240A, C14&H246A, and C14&R240A&H246A mutants were cloned using a NEBuilder HiFi DNA assembly reaction kit in accordance with the manufacturer's instructions. These proteins were expressed in *E. coli* BL21 (DE3) cells and purified. After nickel chelate affinity chromatography, the proteins were further treated with SUMO protease and purified through size exclusion chromatography on a Superdex 200 column in Tris buffer (10 mM Tris/Cl, 200 mM

NaCl, pH8.0). For BphPs assembled in vitro, apoproteins were incubated in darkness in a 10-fold molar excess of BV (Sigma, USA) at room temperature for 1 h. Subsequently, proteins were separated from the free BV by using a DP-10 desalting column (GE Healthcare, USA). The covalent attachment of BV to *Mm*BphP and mutant proteins was monitored through the zinc-induced fluorescence of the chromoproteins subjected to SDS-PAGE. Blue native PAGE was performed on a natural PAGE gel consisting of 3.5% stack and 10% gradient separation gel. The cathode buffer and the anode were cooled at 4°C before it was used. Electrophoresis was started at 80 V for 30 min, increased to 120 V for 1 h, and adjusted to 200 V for 1 h (Li et al. 2019). Covalent attachment of bilins to *Mm*BphP and mutants were monitored by zinc-induced fluorescence of the chromoproteins separated by SDS-PAGE. When purified *Mm*BphP was resolved on SDS-PAGE gels and incubated with 1.5 M zinc acetate, it was visible under ultraviolet light as an orange fluorescent band (Berkelman and Lagarias. 1986). The fluorescent biliprotein-containing bands were visualized by transilluminating the gel on an AlphaImager HP UV light (365 nm) box.

Genetic manipulation of AMB-1

The in-frame deletion of *bphP* was created with a CRISPR-Cas9 system by using the pCRISPomyces-2 plasmid as previously described (Cobb et al. 2015). A sgRNA cassette was designed and inserted into the pCRISPomyces-2 by *Bbs*I site. PCR was performed using PrimerSTAR HS DNA polymerase (Takara, Japan) to amplify 1.0 kb upstream of the start codon in the coding region, and the 1.0 kb sequence downstream of the stop codon and to delete *bphP*. These fragments were then incorporated into an *Xba*I -digested pCRISP-sgRNA vector by using the NEBuilder HiFi DNA assembly reaction system (NEB, USA).

The pCRISP-sgRNA*bphP*-mutant plasmid was constructed as follows. $bphP^{C14A\&R240A\&H246A}$, 1.0 kb upstream sequence, and 1.0 kb downstream sequence were PCR amplified using PrimerSTAR HS DNA polymerase (Takara, Japan). The resulting 3.5 kb fragment was incorporated into the pET28a plasmid. The sgRNA sequence in

the *bphP*$^{C14A\&R240A\&H246A}$ fragment was subjected to nonsense mutation to prevent the sgRNA of the CRISPR plasmid from editing the inserted *bphP*$^{C14A\&R240A\&H246A}$. The resulting plasmid was subjected to site-directed mutagenesis in accordance with the NEBuilder HiFi DNA assembly reaction protocol to introduce the sgRNA sequence of nonsense mutation (sgRNA sequence: GGACTCGCAGCGTTGTACTA to GGACTCGgcGCGTTGTACTA) into the *bphP* sequence. The site-directed 3.5 kb fragment was inserted into pCRISPR-sgRNA*bphP* plasmid with the NEBuilder HiFi DNA assembly reaction system.

The complementing vector ComBphP was constructed through PCR amplification with PrimerSTAR HS DNA polymerase (Takara, Japan). The ComBphP coding sequence was amplified and ligated into *Eco*RI- and *BamH*I-digested pAK0994, a pBBR1MCS-based plasmid carrying a kanamycin resistance gene and expressing the *amb0994-gfp* fusion from a tac promoter. This method was performed as described previously (Chen et al. 2018).

All the plasmids were mobilized into AMB-1 through conjugation with the *E. coli* strain WM3064, and CRISPR-based double-crossover events for deletions or allelic exchange were employed using a selection and screening strategy as described previously (Chen et al. 2018). All the deletions were verified through PCR and sequencing. All the plasmids and primers used are listed in Tables S1 and S2.

Spectroscopic characterization

The absorbance spectra of the purified *Mm*BphP wild-type (WT) and mutant proteins were obtained at room temperature from 850 nm to 250 nm by using a UV-visible spectrophotometer (Unico UV-2800, USA). The assay was recorded either in the dark or after 15 min of illumination with 625 nm, 680 nm, 710 nm, or 750 nm LED light with a half-width of 30 nm at 10 μmol photons/m^2/s (Hasunopto, China). Fig. S1 shows the spectra of these light sources. Dark recovery kinetic was followed at 708 nm and 753 nm after 15 min under 710 nm light. For dark conversion, the half-life time was

estimated as the time in which 50% of the Pfr-to-Pr conversion took place considering the saturation value as 100%. The two phase association exponential fit was used to derive the half-life parameter. Room-temperature fluorescence emission and excitation spectra were recorded using a fluorescence spectrophotometer (Hitachi F-4500, Japan). Fluorescence spectra were obtained at 680 nm excitation or 750 nm emission.

Phototactic behaviour analyses of AMB-1

Phototactic behaviour was quantitatively analyzed as previously described (Li et al. 2017). Using a modified mini MTB collection vessel, the cultures with or without H_2O_2 induction were pooled into the reservoir that is connected to the collecting tube at one side. And then the device was placed in a cassette, where the collection tube was exposed parallelly to the light beam. Before conducting the phototactic experiment, a microaerobic band formed after growing in the dark for 30 min. The upper interface of the microaerobic zone is parallel to the collection tube. After 30 min of 710 nm or 750 nm light irradiation, the OD in the collecting tube and the reservoir was measured ($OD_{collecting\ tube}$ and $OD_{reservoir}$, respectively). The relative numbers of phototactic cells were analyzed by the ratio of ($OD_{collecting\ tube}$ - $OD_{reservoir}$)/$OD_{reservoir}$. Control experiments were performed in the dark. In this study, we analyzed the effect of H_2O_2 on the photoresponse between WT and mutants. To prevent the difference in photoresponse caused by H_2O_2 on the state of bacterial movement for WT and mutants, we observed that at 40 μM concentrations H_2O_2 affected nonsignificantly the velocities of these strains (Fig. S2, Supporting Information). Thus, we studied the difference in phototactic behaviour between the WT and mutants under the conditions of without or with 40 μM H_2O_2. The statistical analyse of phototactic behaviour was conducted through Mann–Whitney *U*-test using SPSS 22.0 (SPSS, IBM).

Results

Identification of BphP

According to the composition of the C-terminal OTD, the domain organization of BphPs can be classified into nine types (Fig. 1A). Three of them (e, f and h) are found

in freshwater AMB-1, MSR-1, MS-1, XM-1, MV-1 or marine QH-2 MTB. Interestingly, BphP proteins in some of these MTB are found to be type (h) BphP which lack the C-terminal OTD (Fig. 1B). The representative *Mm*BphP in the model strain AMB-1 of *Magnetospirillum* sp. consists of a 496 aa PAS–GAF–PHY domain (Fig. 1B). Fig. 1C shows the arrangement of the genes located downstream or upstream of *Mm*BphP in AMB-1, revealing a heme oxygenase gene close to *Mm*BphP. The heme oxygenase opens the heme ring to form the linear tetrapyrole BV which is the first intermediate in phytochrome chromophore synthesis (Muramoto et al. 1999), suggesting *Mm*BphP may be combined with BV in its natural state to perform its functions. Accordingly, by taking AMB-1 as the research object, we studied the possible involvement of BphP with no recognizable OTDs in the photoresponse regulation in MTB. To further enrich the function assessment of BphPs lacking OTDs, we purified the *Mm*BphP protein and constructed the *Mm*BphP deletion mutant in AMB-1 strain.

Characteristics and photochemical properties of recombinant *Mm*BphP protein

Recombinant *Mm*BphP was detected through SDS–PAGE electrophoresis, and a single band migrating at ~54 kDa was observed (Fig. S3 B, Supporting Information). According to the peak position of the elution profiles of a Superdex 200 size-exclusion column, *Mm*BphP displayed a molecular weight of approximately 108 kDa, suggesting the dimer property of these proteins in the solution (Fig. S3 A, Supporting Information). Blue native electrophoresis results revealed that the protein could form stable homodimers (Fig. S3 B, Supporting Information).

In Fig. 2, the purified *Mm*BphP binding to the BV chromophore appears blue green (insert in Fig. 2A). The absorption spectrum of the dark-adapted *Mm*BphP sample is typical of the Pr ground state with a main band centered at 708 nm (Fig. S4, Supporting Information). Illumination of the Pr state with 625 nm, 680 nm or 710 nm light induces only a small absorption increase in the near infra-red region around 753 nm (Fig. 2A; Fig. S4, Supporting Information), which is similar to the ‘Meta’ state of Agp1 BphP

(Borucki et al. 2005), an intermediate during the dark transition from Pfr to Pr. The photoconversion properties of WT *Mm*BphP obtained by these three light treatments are similar. The calculated difference spectrum of *Mm*BphP further shows the characteristic phytochrome signature with maxima of 706 and 753 nm for the two different forms. Irradiation with far-red light (750 nm) results in a spectrum similar to that of the dark-adapted protein (Fig. S4, Supporting Information). The reason of the spectrum change is the rotation of 4th ring D of BV caused by photoisomerization after absorption of red light (Gourinchas et al. 2019). In this study, the 710 nm light was used as red light illumination, and a 750 nm light was used as far-red illumination source.

To assess whether *Mm*BphP has similar structural characteristics as other BphPs, we constructed a predictive structural model of *Mm*BphP using a homologue protein (PBD code 6FHT) as template through Phyre2 search. As shown in Fig. 2B. Like other BphPs (Yang, et al. 2007; Gourinchas et al. 2019), *Mm*BphP is composed of PAS, GAF, and PHY domains. The enlarged dotted line on the right of the predictive structure, by using AutoDock and PyMOL, shows that *Mm*BphP is associated with a bounded BV.

The occurrence of a fast and near complete reversion to the dark-adapted state in Fig. 2C shows that the absorption kinetics changes at 708 nm or 753 nm after 710 nm illumination treatment. The half-time of the dark recovery is 7.8 s at 25°C (Table 1) and several orders of magnitude faster than those reported in phytochromes or BphPs in which dark recoveries occur in periods ranging from minutes to days (Karniol and Vierstra 2003). However, a faster dark recovery than *Mm*BphP has been reported for *Br*BphP3 in *Rhizobium* ORS278 that shows a half-time of 460 ms in dark recovery after illumination (Jaubert et al. 2007).

To further investigate the photochemical characteristics of *Mm*BphP, we analyzed the fluorescent properties of this protein. Fluorescence spectra were obtained at 680 nm excitation or 750 nm emission. Fig. 2D shows the excitation (black line) and emission (gray line) spectra for a suspension of *Mm*BphP recorded at room temperature. The

fluorescence excitation spectra of *Mm*BphP closely match the absorption spectra at 708 nm. The fluorescence emission spectra are centered at 723 nm, which indicates that the fluorescent originates from the BphP-bound BV chromophore (Toh et al. 2011). Similar to the emission spectra of *Mm*BphP, *Dr*BphP emits fluorescence in the near-infrared region at 720 nm, which is substantially longer than the wavelength emitted by GFP-derived fluorescent proteins (Shu at al. 2009).

Identification of *Mm*BphP variants unable to bind to BV

In general, a conserved Cys is in the PAS domain in most bacteria, or in GAF domain in cyanobacterial and plant phytochromes forms the covalent linkage to the bilin chromophore (Kreslavski et al. 2018). To determine the Cys residues involved in covalent attachment to the bilin chromophore in AMB-1, we carried out site-directed mutant experiments (C14A, C211A, C275A, and C291A). In addition AMB-1 BphP residues D197, R240, H245, Y249, S260, and H276, which are conserved to those interacting with the propionate side chains of BV in *Rhodopseudomonas palustris* (Yang, et al. 2007), were also substituted for alanine to analyze their potential binding to BV (Fig. S5 A, Supporting Information).

The binding of BV to WT or mutated AMB-1 *Mm*BphP was analyzed by a zinc-induced fluorescence assay. As demonstrated by zinc-induced fluorescence, apo-*Mm*BphP and all the variants containing C14A show negative results in zinc-induced fluorescence test, confirming the importance of Cys14 for covalently binding to BV (Fig. 3A). To further compare kinetic properties among variants and WT phytochromes, we analyzed the absorption spectroscopy and calculated the half-life time obtained from the experiment that the absorption kinetics changes at 708 nm after 710 nm illumination treatment (Fig. 3B; Table 1). Fig. 3B shows that the absorbance of C14A, D197A or H246A at 708 nm is greatly reduced upon 710 nm light illumination compared with WT. Moreover, the illuminated states possess different life times. The half-life times are 387.9 s, 44.2 s and 5790.1 s for C14A, D197A and H246A, respectively (Table 1). The final photoproduct of these three variants is much longer stable than that of WT.

C211A, R240A, C275A, and C291A exhibit minimal photoconversion and a fast reversion to the dark-adapted state, which is similar to WT. The H276A mutant adopts the Pr dark state but shows no detectable formation of the Pfr state upon illumination at 710 nm. This may result either from completely blocked photoconversion to the Pfr state or from formation of a Pfr state that is too short-lived to be detected in our experiments (Yang et al. 2009). Interestingly, Y249A and S260A resulted in a characteristic of the Pfr state upon 710 nm light illumination and exhibited slower dark recovery compared with WT.

Red light/darkness induced spectral analysis showed that compared with WT protein, C14A could form a photoconvertible holoform with blue-shifted extrema and had detectable absorption at 702 nm in the dark, as well as R240A and H246A (Fig. 3; Table 1). The crystal structures of the chromophore-binding pocket of *Rp*BphP2 and *Rp*BphP3 showed that the Arg240 and His246 residues interact with the propionate side chains of BV (Bellini et al. 2012; Yang et al. 2007). Experimental data confirmed that the H247Q mutation played a role in the stabilization and coordination of the chromophore (Tasler et al. 2005). Fig. 3 shows that the single substitution of these residuces affects zinc-induced fluorescence assay or photochemical spectra at different levels. To assess the accumulation effect of these mutations, we further constructed the double mutants C14&R240 and C14&H246, and the triple mutant C14A&R240A&H246. We observed additional effect of the substitutions, i.e. they almost completely abolished the absorption spectra at 600–800 nm (Fig. 3B).

The Pr and Pfr states of BphPs typically display maximum absorption peaks at approximately 700 nm and 750 nm, respectively, with some overlap in the region between the two peaks. To avoid cross excitation, the red-light sources used to illuminate Pr state are shifted towards lower wavelengths from the maximum absorption peak to 625 nm or 680 nm in order to avoid excitation of the Pfr state. However, for some BphPs that the Pr state displays an absorbance maximum at 700–710 nm, some researchers used 700 nm or 705 nm LED light for red light illumination of Pr, and 750 nm for Pfr (Giraud et al. 2005; Fixen et al. 2014). We compared spectra

of WT *Mm*BphP or mutants illuminated at 710 nm with those at 625 nm, 680 nm or 750 nm. The spectra results by using 625 nm, 680 nm, and 710 nm light sources were similar (Fig. S4, Supporting Information; Fig. S6, Supporting Information). Therefore, we reported the results obtained using LEDs at 710 nm as red light illumination, and 750 nm as far-red illumination source in most case except otherwise specified in this study.

Analysis of phototactic behaviour in AMB-1

Previously we reported that illumination triggers cells to swim toward a light source and helps cells to eliminate intracellular ROS in AMB-1 (Chen et al. 2011; Li et al. 2017). In addition, research reveals that *Rp*BphP4 is redox sensitive (Vuillet et al. 2007). To investigate the effect of *Mm*BphP on phototactic response, we constructed mutant strains and analyzed the phototactic behaviour with or without H_2O_2 in AMB-1 cells by using a modified MTB collection vessel (Chen et al. 2020; Li et al. 2017). The phototactic behaviour was analyzed by illuminating with 710 nm and 750 nm light sources. For AMB-1 WT and mutant strains, the relative number of cells swimming toward 710 nm or 750 nm light was significantly higher ($p<0.01$) than that under the dark condition (Fig. 4). Moreover, for the 710 nm illumination and H_2O_2 treatment groups, the photoresponse of ΔBphP or BphP$^{C14A\&R240A\&H246A}$ mutant cells was significantly weaker than that of WT cells (Fig. 4, $p<0.01$). In contrast, for 750 nm illumination and H_2O_2 treatment groups, there was no significant difference in the phototactic behaviour between WT and mutant cells ($p>0.05$). For strains without H_2O_2 treatment, the number of WT cells swimming toward light was not significantly different from that of the mutant strain ($p>0.05$). In addition, there was no significant difference in the phototactic response between WT and ComBphP cells ($p>0.05$).

Discussion

Photosensing proteins play key roles in the regulation of physiological activities in response to light, a critical element in the acclimatization to the environment. In this study, we described the properties of photosensing protein *Mm*BphP, a new type of

BphPs, presenting in the MTB model strain AMB-1. *Mm*BphP has red/far-red-light-induced photoreversibility features among all members of the phytochrome superfamily. The characteristic absorbance spectra and photoconversion of *Mm*BphP reflect its association with BV chromophore, which are covalently attached at the conserved Cys14 in the PAS domain as most BphPs and Fugal phytochromes do, while plant and cyanobacterial phytochromes are covalently attached at a conserved Cys in the GAF domain. BV adopts the special conformation in the Pr state through the vinyl group of ring A linking to the cysteine covalently and goes through an isomerization at its C15-C16 double bond upon light activation, which results in rotation of ring D (Gourinchas et al. 2019). The *Mm*BphP protein lacking the C-terminal part showed a fast recovery to the stable state after illumination. Our result is consistent with previous findings that the dark recovery is fast in BphPs lacking C-terminal region. *Br*BphP3 lacking natural C-terminal region in *Rhizobium* ORS278 showed a fast dark recovery with half-life time of 460 ms (Jaubert et al. 2007). In *Agrobacterium tumefaciens* and *Xanthomonas campestris*, the Agp2 variant lacking the output module and *Xcc*BphP lacking the PAS9 domain showed much faster kinetics, pointing to the modulation of the dark reversion of the chromophore by the output module (Velazquez et al. 2015; Otero et al. 2016).

In addition, our results showed that light induced photoconversion had a small absorption increase in the near infra-red region around 753 nm, and long-term irradiation would not affect these absorption spectra (data not shown). An obvious Pfr state could not be fully detected in various conditions assayed in this study. We speculate *Mm*BphP may experience a 'fast' Pfr reaction, which evolved on a picosecond or microsecond time scale (Heyne et al. 2002; Jaubert et al. 2007; Singer et al. 2016). This may result from formation of an obvious Pfr state that is too short-lived to be detected in our experiments. Another possibility is that a supplementary protein or component in AMB-1 cells is involved in controlling Pfr to Pr conversion and they are absent in hetero-expressed and purified recombinant *Mm*BphP protein complex. Nevertheless, we do have observed a rapid absorption kinetics change at 708 nm or 753

nm after 710 nm illumination treatment in Fig. 2C, which indicates the occurrence of photoconversion in *Mm*BphP after irradiation.

In the spectral measurement (Fig. 3B; Table 1), substitution of Cys14, Asp197 or His246 exhibited a significantly weakened and broadened absorption band in the red, and detected a slower dark recovery upon 710 nm light illumination compared with WT, suggesting their possibility of being the BV binding pocket which is lined by many highly conserved residues in *Mm*BphP. Alanine substitutions at Cys211, Cys275, and Cys291 show Pr/Pfr photoconversion efficiency similar to the WT *Mm*Bphp, demonstrating the variants could still covalently bind to BV and exhibit a little effect on BV configuration or photoconversion. Moreover, the maximum absorption peaks of C14A, R240A and H246A mutants showed a blue shift of 6 nm to 702 nm in the dark state, indicating that they may affect the binding to BV. Strikingly, illumination of red light on single mutant Y249A and S260A resulted in the appearance of an obvious absorption band (753 nm), characteristic of the Pfr state. These two mutants underwent reversible Pr/Pfr photoconversion, but its rate of reversion to the Pr state in the dark is significantly slower than that of WT, with a half-life time of about 247.8 s and 411.5 s, respectively. Thus, introduction of a single alanine residue into the location of Tyr249 or Ser260 in *Mm*BphP was sufficient to replace the photoconversion of WT *Mm*BphP, suggesting Tyr249 and Ser260 may locate at the binding pocket of *Mm*Bphp, which has a direct impact on the Pr/Pfr photoconversion. Photoconversion of the H276A, is barely detectable in our experiments, but it has normal Pr absorption spectra in the dark. The phenotype indicates that it is likely to be involved in engaging the GAF domain for photoconversion, as the residue in the GAF domain usually interact with the chromophore primarily (Yang et al. 2007). The spectral properties of the variants tested can be noncovalent associations with BV. Because photoconversion does not appear to take covalent attachment as the prerequisite, covalent attachment may provide a more stable holoprotein that make phytochrome suited to reversible photoswitching better by utilize bilin chromophores (Rockwell et al. 2006). In addition to the output module affecting dark recovery (Velazquez et al. 2015; Otero et al. 2016), our results suggest

that the amino acids at the BV binding pocket also affect Pr/Pfr photoconversion efficiency.

Interestingly, BphP$^{C14A\&R240A}$, BphP$^{C14A\&H246A}$ or BphP$^{C14A\&R240A\&H246A}$ exhibited little red, far-red, or near-red absorption and failed to covalently bind to BV, indicating the importance of Cys14, Arg240 and His246 forming the BV binding pocket to some extent. The substitution of arginine with alanine, which abolishes two salt bridges that form with the propionate side chain of the B pyrrole ring, is sufficient to prevent the covalent and noncovalent association of BV with *Rp*BphPs (Fixen et al. 2014). Thus, the conserved arginine in *Mm*BphP may be required for the autocatalytic incorporation of BV. The histidine was characterized to be of important for the chromophore attachment in *Calothrix* sp. PCC7601 CphB (Quest and Gartner 2004). H247Q mutation in *Pseudomonas aeruginosa* resulted in a spectral shift of the Pr and Pfr forms. This result suggested that these mutations play a role in the stabilization and coordination of the chromophore (Tasler et al. 2005). In comparison with the other BphPs, these different characteristics observed in these variants of *Mm*BphP may be related to an increase in the number of hydrogen bonds in the BV-binding pocket, which increases the rigidity of the BV environment (Fixen et al. 2014).

Currently, studies have shown that ultraviolet radiation and free-iron-generated ROS have been major environmental challenges in life on early Earth. Therefore, the initial biomineralization of iron nanoparticles in early life cells has developed into a mechanism to reduce the toxicity of ROS (Lin et al. 2019). Li et al. (2017) found that light helps to eliminate intracellular ROS in AMB-1 cells. Fei et al. (2019) reported that phytochrome A and phytochrome B can help reduce ROS in the cell and are potent regulators of plant defense. Our result showed that under the oxidative stress of H_2O_2 treatment, the number of WT cells moving toward 710 nm light is significantly higher than that of *Mm*BphP mutant strains, while the phototactic behaviour has no significant difference between WT and mutants by illuminating with 750 nm light. The result indicates *Mm*BphP can respond to red light to activate antioxidant enzymes such as

catalase and peroxidase when transformation of Pr into Pfr occurred (Kreslavski et al. 2018), and further help fight toxic effects of oxidative stress or ROS, allowing WT cells to swim toward the light source. The lacking C-terminal region results in a 'classical' output module missing, one may, however, consider *Mm*BphP a genuine photochrome because of the properties of photo response shown in this study. The mechanism of how the C14, R240, H246 affect the photoconversion behaviours through interaction with BV configurations (Fig. S5 B, Supporting Information) and how *Mm*BphP are involved in the light transduction pathway need further study.

Supplementary data

Supplementary data are available at *FEMSLE* online

Acknowledgements

We thank Changyou Chen with the help of useful discussion and suggestions.

Author contributions

The manuscript was written through contributions of all authors. All authors have given approval to the final version of the manuscript. HC, L-FW and TS conceived and designed the experiments. HC, DL and YC prepared samples and carried out the experiment. HC, L-FW and TS reviewed, analyzed and interpreted data. HC and TS wrote the paper and all authors discussed the results and commented on the manuscript.

Funding

This work was supported by the State Key Program of National Natural Science of China (Grant No. 51937011), the National Youth Foundation of China (Grant No. 51907192), the Research Project Funded by the Institute of Electrical Engineering, Chinese Academy of Sciences (Grant No. Y650141CSA), and CNRS-CAS for LIA-MagMC.

Competing interests

The authors declare no conflict of interest.

References

Bai YN, Rottwinkel G, Feng J *et al*. Bacteriophytochromes control conjugation in *Agrobacterium fabrum*. *J Photochem Photobiol B* 2016;**161**:192-9.

Bellini D, Papiz MZ. Dimerization properties of the *Rp*BphP2 chromophorebinding domain crystallized by homologue-directed mutagenesis. *Acta Crystallogr D Biol Crystallogr* 2012; **68**:1058-66.

Berkelman TR, Lagarias JC. Visualization of bilin-linked peptides and proteins in polyacrylamide gels. *Anal Biochem* 1986;**156**:194-201.

Bjorling A, Berntsson O, Lehtivuori H *et al.* Structural photoactivation of a full-length bacterial phytochrome. *Sci Adv* 2016;**2**:e1600920.

Blumenstein A, Vienken K, Tasler R *et al.* The aspergillus nidulans phytochrome FphA represses sexual development in red light. *Curr Biol* 2005;**15**:1833-8.

Bonomi HR, Toum L, Sycz G *et al. Xanthomonas campestris* attenuates virulence by sensing light through a bacteriophytochrome photoreceptor. *EMBO Rep* 2016;**17**: 1565-77.

Borucki B, von Stetten D, Seibeck S *et al.* Light-induced proton release of phytochrome is coupled to the transient deprotonation of the tetrapyrrole chromophore. *J Biol Chem* 2005;**280**:34358-64.

Brutesco C, Prévéral S, Escoffier C *et al*. Bacterial host and reporter gene optimization for genetically encoded whole cell biosensors. *Environ Sci Pollut Res Int* 2017;**24**:52-65.

Burgie ES, Zhang J, Vierstra RD. Crystal Structure of *Deinococcus* phytochrome in the photoactivated state reveals a cascade of structural rearrangements during photoconversion. *Structure* 2016;**24**:448-57.

Chen CF, Ma QF, Jiang W *et al.* Phototaxis in the magnetotactic bacterium *Magnetospirillum magneticum* strain AMB-1 is independent of magnetic fields. *Appl Microbiol Biotechnol* 2011;**90**:269-75.

Chen HT, Li KF, Cai Y *et al.* Light regulation of resistance to oxidative damage and

529 magnetic crystal biogenesis in *Magnetospirillum magneticum* mediated by a
530 Cys-less LOV-like protein. *Appl Microbiol Biotechnol*
531 2020;https://doi.org/10.1007/s00253-020-10807-5.
532 Chen HT, Zhang S-D, Chen LJ *et al.* Efficient genome editing of *Magnetospirillum*
533 *magneticum* AMB-1 by CRISPR-Case9 system for analyzing magnetotactic
534 behavior. *Front Microbiol* 2018;**9**:1569-81.
535 Chen YR, Zhang R, Du HJ *et al.* A novel species of ellipsoidal multicellular
536 magnetotactic prokaryotes from Lake Yuehu in China. *Environ Microbiol*
537 2015;**17**:637-47.
538 Cobb RE, Wang Y, Zhao H. High-efficiency multiplex genome editing of *Streptomyces*
539 species using an engineered CRISPR/Cas system. *ACS Synth Biol* 2015;**4**:723-
540 8.
541 de Melo RD, Acosta-Avalos D. Light effects on the multicellular magnetotactic
542 prokaryote '*Candidatus* Magnetoglobus multicellularis' are cancelled by
543 radiofrequency fields: the involvement of radical pair mechanisms. *Antonie van*
544 *Leeuwenhoek* 2017;**110**:177-86.
545 Duanmu D, Bachy C, Sudek S *et al.* Marine algae and land plants share conserved
546 phytochrome signaling systems. *Proc Natl Acad Sci U S A* 2014;**111**:15827-32.
547 Faivre D, Schüler D. Magnetotactic bacteria and magnetosomes. *Chem Rev*
548 2008;**108**:4875-98.
549 Fei CY, Chen LY, Yang T *et al.* The role of phytochromes in *Nicotiana tabacum* against
550 *Chilli veinal mottle virus*. *Plant Physiol Biochem* 2019;**139**:470-7.
551 Fixen KR, Baker AW, Stojkovic EA *et al.* Apo-bacteriophytochromes modulate
552 bacterial photosynthesis in response to low light. *Proc Natl Acad Sci U S A*
553 2014;**111**:E237-E44.
554 Frankel RB, Bazylinski DA, Johnson MS *et al.* Magneto-aerotaxis in marine coccoid
555 bacteria. *Biophys J* 1997;**73**:994-1000.
556 Frankel RB, Blakemore RP. Magnetite and magnetotaxis in microorganisms.
557 *Bioelectromagnetics* 1989;**10**:223-37.
558 Giraud E, Zappa S, Vuillet L *et al.* A new type of bacteriophytochrome acts in tandem

559 with a classical bacteriophytochrome to control the antennae synthesis in
560 *Rhodopseudomonas palustris*. *J Biol Chem* 2005;**280**: 32389-32397.
561 Gomelsky M, Hoff WD. Light helps bacteria make important lifestyle decisions. *Trends*
562 *Microbiol* 2011;**19**:441-8.
563 Gourinchas G, Etzl S, Winkler A. Bacteriophytochromes-from informative model
564 systems of phytochrome function to powerful tools in cell biology. *Curr Opin*
565 *in Struct Biol* 2019;**57**:72-83.
566 Heyne K, Herbst J, Stehlik D *et al.* Ultrafast dynamics of phytochrome from the
567 *Cyanobacterium Synechocystis*, reconstituted with phycocyanobilin and
568 phycoerythrobilin. *Biophys J* 2002; **82**:1004-16.
569 Hughes J, Lamparter T, Mittmann F *et al.* A prokaryotic phytochrome. *Nature*
570 1997;**386**:663.
571 Jaubert M, Lavergne J, Fardoux J *et al.* A singular bacteriophytochrome acquired by
572 lateral gene transfer. *J Biol Chem* 2007;**282**:7320-8.
573 Jaubert M, Vuillet L, Hannibal L *et al.* Control of peripheral light-harvesting complex
574 synthesis by a bacteriophytochrome in the aerobic photosynthetic bacterium
575 *Bradyrhizobium* strain BTAi1. *J Bacteriol* 2008;**190**:5824-31.
576 Jiang ZY, Swem LR, Rushing BG *et al.* Bacterial photoreceptor with similarity to
577 photoactive yellow protein and plant phytochromes. *Science* 1999;**285**:406-9.
578 Karniol B, Vierstra RD. The pair of bacteriophytochromes from *Agrobacterium*
579 *tumefaciens* are histidine kinases with opposing photobiological properties.
580 *Proc Natl Acad Sci U S A* 2014 2003;**100**:2807-12.
581 Karniol B, Vierstra RD. The HWE histidine kinases, a new family of bacterial two-
582 component sensor kinases with potentially diverse roles in environmental
583 signaling. *J Bacteriol* 2004;**186**: 445-53.
584 Karniol B, Wagner JR, Walker JM *et al.* Phylogenetic analysis of the phytochrome
585 superfamily reveals distinct microbial subfamilies of photoreceptors. *Biochem*
586 *J* 2005;**392**:103-16.
587 Kelley LA, Mezulis S, Yates CM *et al.* The Phyre2 web portal for protein modeling,
588 prediction and analysis. *Nat Protoc* 2015;**10**:845-58.

589 Kreslavski VD, Los DA, Schmitt F-J *et al.* The impact of the phytochromes on
590 photosynthetic processes. *Biochim Biophys Acta Bioenerg* 2018;**1859**:400-8.
591 Lamparter T, Carrascal M, Michael N *et al.* The biliverdin chromophore binds
592 covalently to a conserved cysteine residue in the N-terminus of *Agrobacterium*
593 *phytochrome* Agp1. *Biochemistry* 2004;**43**:3659-69.
594 Li DD, Wang J, Jin Z *et al.* Structural and evolutionary characteristics of dynamin-
595 related GTPase OPA1. *Peer J* 2019;**7**: e7285.
596 Li KF, Wang PP, Chen CF *et al.* Light irradiation helps magnetotactic bacteria eliminate
597 intracellular reactive oxygen species. *Environ Microbiol* 2017;**19**:3638-48.
598 Lin W, Kirschvink JL, Paterson GA *et al.* On the origin of microbial magnetoreception.
599 *Natl Sci Rev* 2019;**7**:472-9.
600 Lin W, Paterson GA, Zhu QY *et al.* Origin of microbial biomineralization and
601 magnetotaxis during the Archean. *Proc Natl Acad Sci U S A* 2017;**114**:2171-6.
602 Maresca JA, Keffer JL, Hempel PP *et al.* Light modulates the physiology of
603 *Nonphototrophic Actinobacteria*. *J Bacteriol* 2019;**201**:e00740-18.
604 Matsunaga T, Sakaguchi T, Tadokoro F. Magnetite formation by a magnetic bacterium
605 capable of growing aerobically. *Appl Microbiol Biotechnol* 1991;**35**:651-5.
606 Moyano L, Carrau A, Petrocelli S *et al.* Bacteriophytochromes from *Pseudomonas*
607 *syringae* pv. *tomato* DC3000 modulate the early stages of plant colonization
608 during bacterial speck disease. *Eur J Plant Pathol* 2020; doi:10.1007/s10658-
609 019-01918-5.
610 Mukherjee S, Jemielita M, Stergioula V *et al*. Photosensing and quorum sensing are
611 integrated to control *Pseudomonas aeruginosa* collective behaviors. *PLoS Biol*
612 2019;**17**: e3000579.
613 Muramoto T, Kohchi T, Yokota A *et al.* The Arabidopsis photomorphogenic mutant *hy1*
614 is deficient in phytochrome chromophore biosynthesis as a result of a mutation
615 in a plastid heme oxygenase. *Plant Cell* 1999;**11**:335-48.
616 Nagano S. From photon to signal in phytochromes: similarities and differences between
617 prokaryotic and plant phytochromes. *J Plant Res* 2016;**129**:123-35.
618 Otero LH, Klinke S, Rinaldi J *et al.* Structure of the full-length bacteriophytochrome

619 from the plant pathogen *Xanthomonas campestris* provides clues to its long-
620 range signaling mechanism. *J Mol Biol* 2016*;* **428**:3702-20.
621 Philippe N, Wu L-F. An MCP-like protein interacts with the MamK cytoskeleton and
622 is involved in magnetotaxis in *Magnetospirillum magneticum* AMB-1. *J Mol*
623 *Biol* 2010;**400**:309-22.
624 Qian XX, Santini CL, Kosta A *et al.* Juxtaposed membranes underpin cellular adhesion
625 and display unilateral cell division of multicellular magnetotactic prokaryotes.
626 *Environ Microbiol* 2019;**22**:1481-94.
627 Quest B, Gartner W. Chromophore selectivity in bacterial phytochromes-Dissecting the
628 process of chromophore attachment. *Eur J Biochem* 2004;**271**:1117-26.
629 Ricci A, Dramis L, Shah R *et al.* Visualizing the relevance of bacterial blueand red-
630 light receptors during plant-pathogen interaction. *Environ Microbiol Rep*
631 2015;**7**:795-802.
632 Rockwell NC, Su Y-S, Lagarias JC. Phytochrome structure and signaling mechanisms.
633 *Annu Rev Plant Biol* 2006a;**57**: 837-58.
634 Rodriguez-Romero J, Hedtke M, Kastner C *et al.* Fungi, Hidden in soil or up in the air:
635 Light makes a difference in: Gottesman S, Harwood CS (eds.) *Annu Rev*
636 *Microbiol* 2010;**64:**585-610.
637 Rottwinkel G, Oberpichler I, Lamparter T. Bathy phytochromes in rhizobial soil
638 bacteria. *J Bacteriol* 2010;**192**:5124-33.
639 Shapiro OH, Hatzenpichler R, Buckley DH *et al.* Multicellular photo-magnetotactic
640 bacteria. *Environ Microbiol Rep* 2011;**3**:233-8.
641 Shu XK, Royant A, Lin MZ *et al*. Mammalian expression of infrared fluorescent
642 proteins engineered from a bacterial phytochrome. *Science* 2009 **324**:804-807.
643 Singer P, Worner S, Lamparter T *et al.* Spectroscopic investigation on the primary
644 photoreaction of bathy phytochrome Agp2-Pr of *Agrobacterium fabrum*:
645 isomerization in a pH-dependent H-bond network. *Chem Phys Chem* 2016;**17**:
646 1288-97.
647 Tasler R, Moises T, Frankenberg-Dinkel N. Biochemical and spectroscopic
648 characterization of the bacterial phytochrome of Pseudomonas aeruginosa. *Febs*

649 *Journal* 2005;**272**:1927-36.
650 Toh KC, Stojković EA, van Stokkum IHM *et al.* Fluorescence quantum yield and
651 photochemistry of bacteriophytochrome constructs. *Phys Chem Chem Phys*
652 2011;**13**:11985.
653 Velazquez EF, Piwowarski P, Salewski J *et al*. A protonation-coupled feedback
654 mechanism controls the signalling process in bathy phytochromes. *Nat Chem*
655 2015; **7**: 423-30.
656 Vuillet L, Kojadinovic M, Zappa S *et al.* Evolution of a bacteriophytochrome from light
657 to redox sensor. *Embo Journal* 2007;**26**: 3322-31.
658 Wang YZ, Casaburi G, Lin W *et al*. Genomic evidence of the illumination response
659 mechanism and evolutionary history of magnetotactic bacteria within the
660 Rhodospirillaceae family. *BMC genomics* 2019;**20**: 407.
661 Wu L, McGrane RS, Beattie GA. Light regulation of swarming motility in
662 *Pseudomonas syringae* integrates signaling pathways mediated by a
663 bacteriophytochrome and a LOV protein. *MBio* 2013;**4**: e00334-13.
664 Yang CD, Takeyama H, Tanaka T *et al.* Effects of growth medium composition, iron
665 sources and atmospheric oxygen concentrations on production of luciferase-
666 bacterial magnetic particle complex by a recombinant *Magnetospirillum*
667 *magneticum* AMB-1. *Enzyme Microb Technol* 2001;**29**:13-9.
668 Yang XJ, Kuk J, Moffat K. Conformational differences between the Pfr and Pr states in
669 *Pseudomonas aeruginosa* bacteriophytochrome. *Proc Natl Acad Sci U S A*
670 2009;**106**:15639-44.
671 Yang XJ, Stojkovic EA, Kuk J *et al.* Crystal structure of the chromophore binding
672 domain of an unusual bacteriophytochrome, *Rp*BphP3, reveals residues that
673 modulate photoconversion. *Proc Natl Acad Sci U S A* 2007;**104**:12571-6.
674 Zhou K, Zhang WY, Kui YZ *et al.* A novel genus of multicellular magnetotactic
675 prokaryotes from the Yellow Sea. *Environ Microbiol* 2012;**14**:405-13.
676
677
678 Figures

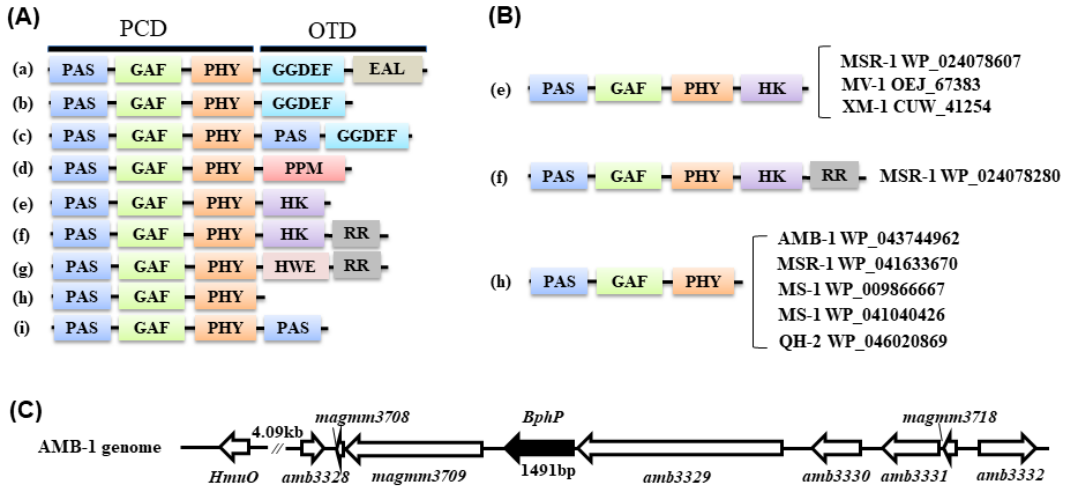

679

680 Fig 1 Domain organization and arrangement of genes for BphPs. (A) The domain
681 organization of BphPs in bacteria can be classified into nine types (a–i). (B) Domain
682 organization of various BphP sequences in MTB. (C) Arrangement of the genes located
683 downstream or upstream of *Mm*BphP in AMB-1. The arrows indicate the direction of
684 transcription. *HmuO* encodes heme oxygenase.

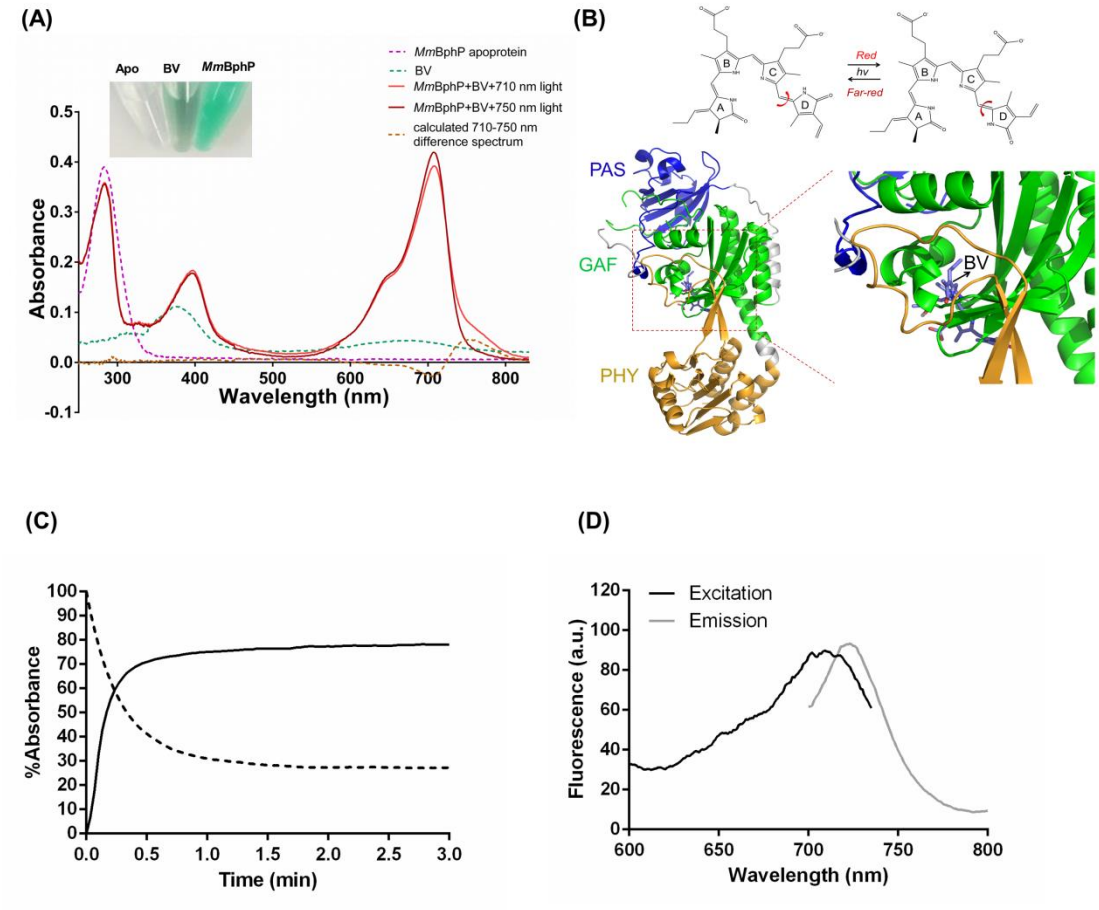

685

686 Fig 2 Biochemical characterization of *Mm*BphP. (A) Absorption spectra of purified
687 *Mm*BphP, *Mm*BphP apoprotein (purple dotted line), BV (green dotted line), after
688 photoconversion with red light (red line, 710 nm) and far red light (dark red line, 750
689 nm), and their difference spectrum (orange dotted line). The insert shows the images of
690 BphP apoprotein, BV and *Mm*BphP with BV binding. (B) The possible molecular
691 configuration of BV used in this work that could be triggered by red or far red light
692 (upper). A predictive structure of *Mm*BphP with BV binding was constructed through
693 Phyre2 search (lower). *Mm*BphP is composed of PAS (blue), GAF (green), and PHY
694 (orange) domains. BV is shown in light blue. (C) Dark reversion of *Mm*BphP after 710
695 nm illumination. Dark recovery kinetic was followed at 708 nm (black line) and at 753
696 nm (dotted line). (D) The fluorescence excitation spectrum (black line) and emission
697 spectrum (gray line) of *Mm*BphP.

698

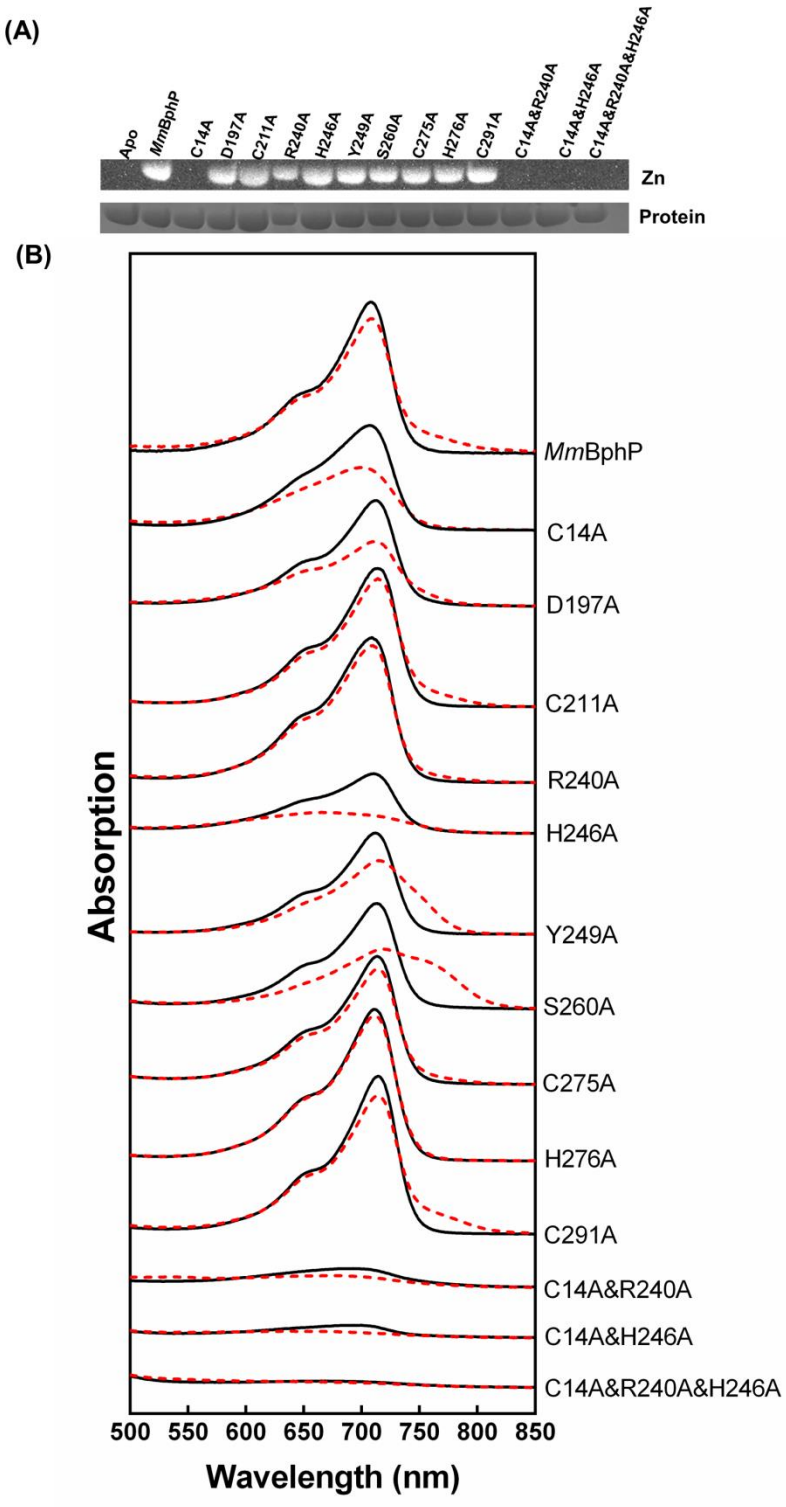

699

700 Fig 3 Zinc-induced fluorescence and absorbance spectra of *Mm*BphP variants. (A)
701 Purified proteins were subjected to SDS-PAGE and assayed for assembly with BV by
702 using a zinc-induced fluorescence assay. (B) Absorption spectra of purified WT and
703 selected mutants of *Mm*BphP. The spectra were obtained for protein incubated in the
704 dark (black line) and after illumination with 710 nm light for 15 min (red dashed line).

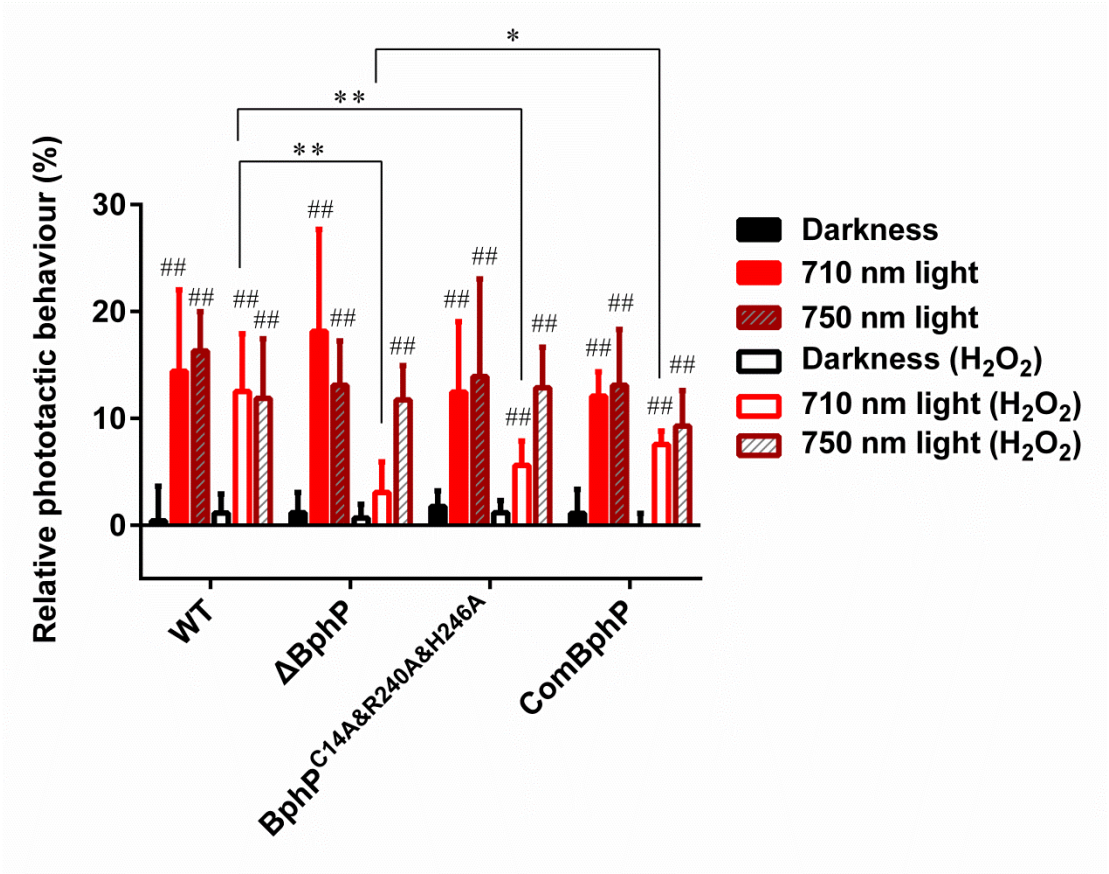

Fig 4 Relative phototactic behaviour (%) of AMB-1 WT cells and mutants (n=5). Bars and error bars depict the mean±SD. Level of significance of the differences observed between light and dark control is expressed as hashtag sign (#p<0.05 and ##p<0.01). The significant differences between the two groups depicted by the lines in the graph are indicated by asterisks (∗p<0.05 and ∗∗p<0.01).

Table 1 The spectral properties of *Mm*BphP variants

Proteins	Absorption spectrum	Half-life time (s)
	Pr λmax (nm)	
*Mm*BphP	708	7.8
C14A	702	387.9
D197A	708	44.2
C211A	708	9.1
R240A	702	14.6

H246A	702	5790.1
Y249A	706	247.8
S260A	708	411.5
C275A	708	11.4
H276A	708	22.3
C291A	708	8.9
C14A&R240A	689	-
C14A&H246A	693	-
C14A&R240A&H246A	-	-

714

715